The fascinating physics of carbon surfaces: first-principles study of hydrogen on C(001), C(111) and graphene

Margherita Marsili, Olivia Pulci

The fascinating physics of carbon surfaces: first-principles study of hydrogen on C(001), C(111), and graphene

Margherita Marsili[1], **Olivia Pulci**[1]

(1) ETSF, CNR-INFM, NAST and Dipartimento di Fisica dell'Università di Roma Tor Vergata, Via della Ricerca Scientifica 1, I-00133 Roma, Italy

Abstract. With the aid of ab-initio, parameter free calculations based on density-functional and many-body perturbation theory, we investigate the electronic band structure and electron affinity of diamond surfaces. We focus on clean, ideal (001) and (111) surfaces, and on the effect of hydrogen adsorption. Also single sheets of graphane, that is graphene functionalized upon hydrogen, are investigated. At full H-coverage nearly-free electron states appear near the conduction band minimum in all the systems under study. At the same time, the electron affinity is strongly reduced becoming negative for the hydrogenated diamond surfaces, and almost zero in graphane. The effects of quasi-particle corrections on the electron affinity and on the nearly free electron states are discussed.

1. Introduction

Diamond is outstanding for its unique bulk properties: it is harder than any other material, and it has the highest thermal conductivity. However, many of the most interesting and potentially useful properties of diamond stem from its surface physics. Despite the fact that diamond, Si and Ge share the same crystal and valence-electron structure, their surface properties such as the most stable reconstructions [1], the details of the geometry, the electronic band structure differ qualitatively and follow a quite clear chemical trend connected to the strength of the covalent bond of the crystal. In many cases, the most interesting phenomena present only at diamond surface are linked to the adsorption of hydrogen [2]. At odds with Si and Ge, C is more electronegative with respect to H. So that, upon hydrogen absorption, a microscopic surface dipole pointing out of the surface is produced. This leads to the lowering of the local vacuum level [3] in such a way that the electron affinity becomes negative [4](for a review see [2]). At the same time the ionization potential of the system becomes the smallest known for any semiconductors and allows for a special type of transfer doping where holes are injected by surface adsorbates that act as acceptors. This process is known as surface transfer doping and leads to high surface conductivity [5, 6].

In this paper we review ab-initio theoretical studies concerning the structure and electronic properties of the most relevant surfaces of diamond, namely C(001) and C(111), clean and hydrogen-covered. Also new results, concerning the electron affinity of these surfaces, will be presented. Just ideal (flat, no defects, no steps) geometries will be here considered. Of course, real surfaces are much more complicated, presenting domains, terraces, and many other unavoidable deviations from the perfect, ideal models we use (see for example [7, 8, 9, 10]). Along with such C surfaces, we will look at the effect of hydrogen coverage on graphene. When hydrogen entirely covers graphene, a new 2D crystal, named graphane, is formed.

Hydrogenation of C surfaces and of graphene brings some common features. First of all hydrogen enhances the semiconducting character of C(100) and is able to open a gap at the density-functional theory (DFT) level concerning C(111) and graphene. Secondly, the presence of hydrogen gives rise to unoccupied states within the fundamental gap close to the Γ point. Some of this states have a nearly-free electron (NFE) character [14]. The peculiar spatial distribution of such states leads up to distinct many-body effects, in particular the quasi-particle shift are strongly reduced with respect to the other conduction states. Finally, both hydrogenated diamond surfaces show a negative electron affinity (NEA), and also graphene undergoes a marked reduction of its electron affinity upon hydrogenation, passing it from several eV to almost zero (although still positive).

The paper is organized as follows: in the next section we will briefly describe the theoretical approaches we use, namely DFT, and the GW approximation for the electronic self-energy. Next, the C(001)2×1 clean and H covered (monohydride phase) will be described. In section IV we will present the state of the art of the knowledge of

the electronic properties of the C(111)2×1 surface, pointing out the still not answered questions. Its hydrogenated phase will also be discussed. Finally, in section V we give a brief overview on some of graphene properties, focussing on its functionalization through H.

2. Computational methods

In this section we shortly introduce the theoretical tools used for the determination of the properties of the studied systems. We will not give a detailed derivation of the employed theories and formulas, leaving the reader to more complete reviews for further insight and information. Instead we aim, here, to elucidate the different physical content captured by theory at each different level of sophistication. This will be done in order to provide the readers with the possibility to correctly interpret the theoretical results presented.

2.1. Ground state properties

All the results presented in this review, take the first step from a DFT calculation. DFT is based on the seminal paper of Hohenberg and Kohn of 1964[18]. For a review on DFT see for example [19]. In their paper, Hohenberg and Kohn proved that all the ground state properties of an interacting electronic system, including the many-body wave function, could be expressed as unique functionals of the electronic density alone. In particular, this assertion is valid also for the total energy E of the system. Moreover, the total energy functional is minimum at the exact ground-state electron density of the system. Customarily, DFT provides insights on the ground state properties of materials and nanostructures through the solution of the so called Kohn-Sham (KS) equations [20]. The main idea underlying this approach is to map the study of the interacting system into the study of a non interacting fictitious system whose Hamiltonian is written as:

$$\{-\frac{1}{2}\nabla^2 + v_{ext} + v_H + v_{xc}\}\phi_i(r) = \epsilon_i^{KS}\phi_i(r) \tag{1}$$

and which has by construction the same ground state density $n(r)$ of the interacting system:

$$n(r) = \sum_i f_i|\phi_i(r)|^2, \tag{2}$$

being f_i the occupation number of the state i. In Eq.1, v_{ext} is the fixed external potential, v_H is the Hartree potential, and v_{xc} is the so called exchange-correlation (xc) potential. It is now possible, given an approximation for v_{xc} (typically local-density approximation (LDA) or generalized-gradient approximation (GGA) [20, 21]), to solve the KS equations (1,2) self-consistently and calculate the density n(r). Once the density is known, it is possible to calculate the energy of the interacting system and hence, by proper minimization, to find its ground state geometry:

$$E_0 = min_{\{n\}}E[n] \tag{3}$$

The KS equations, representing a fictitious auxiliary system, have no physical meaning. Nevertheless, their eigenvalues ϵ_i^{KS} are often interpreted as one electron excitation energies corresponding to the excitation spectra of the system upon removal or addition of an electron. The collection of such eigenvalues gives rise to the so called DFT-KS band structure. Typically, DFT-KS band structures severely underestimate the band gap of semiconductors and insulators. A better description of band gaps and the removal of spurious self-interaction effects (arising from the approximation of the xc potential) can be obtained employing non-local xc potentials in the so called generalised Kohn-Sham scheme [22, 23, 24]. Finally, it is worth mentioning that often in the presence of localised d and f electrons, such as in the so called 'strongly-correlated systems', even the description of the ground-state is unsatisfactory within LDA. Possible methods to overcome this and the band-gap problem include self-interaction corrected LDA [25] and LDA+U method [26]. However for simpler semiconducting systems, such as diamond, DFT-LDA is well suited for the description of the ground-state properties.

2.2. Electronic Band structure calculations beyond DFT

Many-body perturbation theory(MBPT), although computationally cumbersome, is a framework where excited states are straightforwardly and easily approached. Within MBPT, the single particle excitation energies are the poles of the single-particle Green's function G. Such poles are exactly $\varepsilon_n = \pm E_n(N \pm 1) \mp E(N)$ where $E(N)$ is the ground-state energy of the neutral system (containing N electrons) and $E_n(N \pm 1)$ is the energy of the n-th excited state of the charged $N \pm 1$ system. Thus, from the knowledge of the poles of the Green's function, we have direct access to the excitation energies ε_n, which may be compared with direct and inverse photoemission experiments. Also the ionization potential I and the electron affinity χ are easily accessible within the MBPT approach, being the energy of the highest occupied state, and the energy of the lowest unoccupied state, respectively. As a corollary, the electronic gap $E_{gap} = I - \chi$ is also known.

Here we will shortly describe the Green's function theory and the quasi-particle approach. Further information and more details can be found in books of many-particle physics [27].

When a bare particle, like an electron or an hole, is added to an interacting system, it perturbs the particles in its vicinity and is dressed by a polarization cloud of the surrounding particles, becoming a so-called *quasi-particle*. The propagation of the *quasi-particle* within the system is ruled by the so-called "quasiparticle equation":

$$(-\frac{1}{2}\nabla^2 + v_{ext} + v_H)\Psi_i(\vec{r},\omega) + \int \Sigma(\vec{r},\vec{r'},\omega)\Psi_i(\vec{r'},\omega)d\vec{r'} = \varepsilon_i(\omega)\Psi_i(\vec{r}). \quad (4)$$

Besides the external and Hartree potential, the quasi-particles experience also another sort of 'potential', Σ, a non local, time-dependent, non hermitian operator called the *self-energy*. The self-energy takes into account all the interactions and the electronic relaxation beyond the classic Hartree repulsion term. Upon the electron removal

	Γ	X	L	$E_{gap}^{ind}(\Gamma \rightarrow X)$	top valence (Γ)	bottom conduction (Γ)
LDA	5.65	11.27	11.39	4.26	0.0	5.65
GW	7.4	13.0	13.4	5.7	-0.6	6.8
exp.[32]	7.3			5.5		

Table 1. DFT-LDA and GW electronic gaps of diamond at high symmetry points, and absolute values of the top valence and bottom conduction band at the Γ point

(addition), the relaxation of the system will vary depending on the energetic level that is probed (for instance whether the extracted charge belongs to the core or to the valence electrons) and in fact the self-energy is energy-dependent. The quasi-particle states are not, in fact, exact eigen-states of the systems and will decay after a certain time. Being Σ not-hermitian, the energies $\varepsilon_i(\omega)$ are in general complex: their imaginary part is related to the life time of the excited particle [28].

Neglecting vertex corrections [29], the self-energy can be expressed in terms of the single-particle Green's function G, and the screened Coulomb interaction W as:

$$\Sigma(12) = iG(12)W(1^+2); \tag{5}$$

in this equation the notation (1,2) stands for two pairs of space and time coordinates, $(\mathbf{r}_1, t_1; \mathbf{r}_2, t_2)$. This is the so called GW approximation for the self energy.

The omission of vertex correction is not the only approximation that is typically used when the GW method is used. In practical calculations, being the KS equations of the DFT a good starting approximation, both G and W are calculated using the DFT-LDA eigenvalues and eigenfunctions at the independent-particle level this represents the "one-shot" G_0W_0. Moreover, since eq.(1) is formally similar to eq. (4), the self-energy corrections might be evaluated considering the term $(\Sigma - v_{xc}^{DFT})$ as a perturbation term of the KS equations. The first order perturbation approach to calculate the QP energies has been proved to be valid within 0.1-0.2 eV for bulk [30] and surfaces [31]. As an example, we show in Tab. 1 the electronic gaps at the high symmetry points of the Brillouine Zone for diamond bulk. DFT always results in an underestimation of the gaps, and GW corrects them by un upward shift of the empty states and downward shift of the filled states. It is worth to note that the shift is not k-independent, i.e. a 'scissor operator approximation' (meaning a rigid constant shift) would not be justified in diamond.

For what concerns the QP wavefunctions, they result to be well approximated by the DFT on many bulk semiconductor systems [29, 30, 33, 34]. However the situation may be sometimes more complex, since it has been shown [31, 33, 35, 36, 37, 24, 38, 39, 40, 41] that small but sizeable differences between ψ^{QP} and ϕ^{DFT} can occur for some (quasi)particle states.

It is worth to mention that the GW approximation can be seen as a dynamically screened Hartree Fock (HF) approximation. The Hartree Fock equation is exactly recovered if Σ is approximated to $\Sigma = iGV$ with V bare (as opposite to screened) Coulomb potential. It

is well known that the HF approximation, containing just the exchange potential, largely overestimates the electronic gaps in semiconductors (see for example [24]). On the other hand, setting Σ equal to a local, energy independent exchange and correlation potential, would reproduce the DFT Kohn-Sham equations (which systematically underestimate the electronic gaps). In this framework, it is hence intuitive that an improved description of the electronic gaps could come by adding a statically screened non-local exchange potential (sX [22]) to the DFT one. The screened exchange contains the Thomas-Fermi screening constant k_{TF} that is material dependent and may used as an adjustable parameter. As a further advantage, sX is computationally much less heavy than a GW. In this paper we will show that this simplified approach works quite well for the C(001) surface, but fails in the C(111) case.

3. The C(001) surface

In this section we focus on the 001 surface of diamond. This is the technologically most important face, being the smoothest in CVD growth [2]. From the theoretical point of view, it is also the most studied and best understood. At odd with the C(111) surface, in fact, there are no open issues concerning its geometry and electronic band structure.

3.1. Clean surface

As-polished or acid-cleaned C(001) surfaces exhibits a (1x1) low-energy electron diffraction (LEED) pattern. Annealing at temperature higher that 1300 K produces a 2×1 LEED pattern ([42, 43] and reference therein). It is commonly accepted that the C(001)2×1 corresponds to a dimerized geometry. At odd with the Si(001)[44] and Ge(001) [45]-2×1, the C-C dimers are not buckled [2, 17, 46, 47, 48, 49, 50, 51].

Our DFT-LDA calculated geometry, shown in Fig.1, reveals a C dimer bond length of 1.37 Å [52], slightly larger than the C=C double bond (1.31 Å) and smaller than a single bond length (1.58 Å). A small buckling appears just in the layers beneath the two topmost surface layers: the buckling of the 3rd layer is 0.27 Å, the one of the 4th layer 0.16 Å, in agreement with other DFT results (see for example [49, 53] and references therein).

3.1.1. Electronic band structure The electronic band structure, calculated with the inclusion of many-body effects at different levels of approximation [57], is shown in Fig. 2. Direct photoemission data by Graupner et al. [56] are also inserted in the figure (squares symbols). The agreement between theory and experiment is very good, hence validating the theoretical approaches. The surface electronic gaps at high-symmetry points of the irreducible part of the Brillouine zone (IBZ) are listed in Tab. 2. The QP corrections open the LDA gaps between occupied and empty surface states by 1.8-2.1 eV. The GW corrections do not affect much the dispersion of the states, leaving the minimum surface gap indirect (from around J' to K) and the surface bands almost

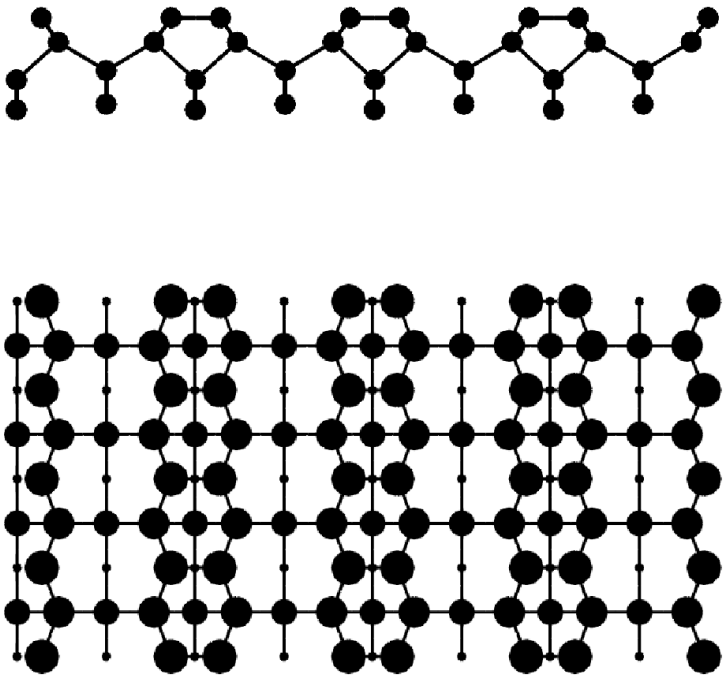

Figure 1. Side and top view of the C(001)2×1 surface. Black balls represent C atoms.

	Γ	J	K	J'
DFT-LDA	2.7	3.2	2.9	2.2
GW [58]	4.8	5.3	5.0	4.0
sX [57]	4.7	5.2	4.9	3.9

Table 2. Electronic gaps (in eV) between surface states in C(001)2×1

parallel near J' (see Fig. 2). This parallelism, together with the low dielectric screening of diamond, is the main reason for the formation of a bound exciton in the optical properties of this surface [51]. Using a simplified GW scheme for the screening, Kress et al. [53] obtained similar results, but a slightly larger opening of the surface state gaps (2.14-2.35 eV). Simplified approaches as screened exchange (sX, [22, 57]) also allow to reproduce the full GW gap.

The calculated electron affinity χ for C(001)2×1 is shown in Tab. 3. In DFT it takes the value of 1.9 eV, out of the experimental range (from 0.5 to 1.3 eV [17, 59, 60]). The inclusion of QP effects allows for a better agreement with the measurements: our GW value for χ, 1.1 eV, falls well within the experimental range. Comparison with other DFT calculations, corrected by using an upward shift of the conduction states

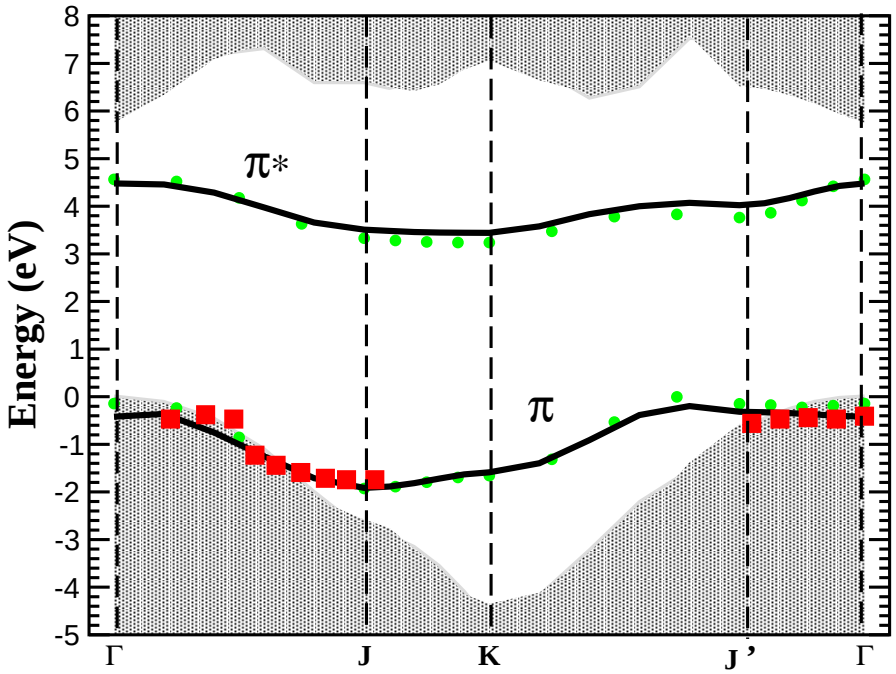

Figure 2. Electronic band structure of (001) surface along high-symmetry lines of the 2×1 BZ. The two surface bands in the gap, corresponding to π and π^* orbitals at the C dimers, are calculated within GW (solid lines) and within sX (circles). Experimental data (squares) from [56].

[49] or corrected by the use of the experimental C bulk gap [61, 55] are also shown in Tab. 3.

	$\chi^{th}_{DFT-LDA}$ [63]	χ^{th}_{GW}[63]	χ^{th}	χ^{exp}
C(001)2 × 1	1.9	1.1	0.51[61], 0.64[49], 0.8[55]	0.5[17], 0.75[59], 1.3[60]
C(001)2 × 1:H	-0.7	-1.5	-2.05[61], -1.90[49], -2.2[55]	∼ -0.8[42], ∼ -0.4[65], ≤ -1.0[60] -1.3[17]
C(111)2 × 1	1.6	0.8	0.35[61], 0.35[49]	1.5 [60], 0.5 [59, 64], 0.38 [62
C(111)1×1:H	-0.6	-1.4	-2.03[61], -1.97[49]	≤ -0.7[64], ≤-0.9 [60], -1.27 [6

Table 3. Theoretical Electron affinity for the clean and hydrogenated (001) and (111) surfaces computed at the DFT and GW level. Also theoretical values (χ^{th}) from [49], [61] and [55] are reported. Experimental data are also shown (χ^{exp}). All energies are in eV.

3.2. C(001)2×1:H

The interaction of hydrogen with diamond surfaces is of large technological interest: high quality diamond films grown via CVD have been obtained by etching with atomic hydrogen at 1000° Celsius [8]; negative electron affinity upon hydrogen adsorption [4] makes diamond a promising candidate as cold cathod emitter. It is hence crucial to get a deeper microscopic insight of the interaction of H with the C(001) surface. The

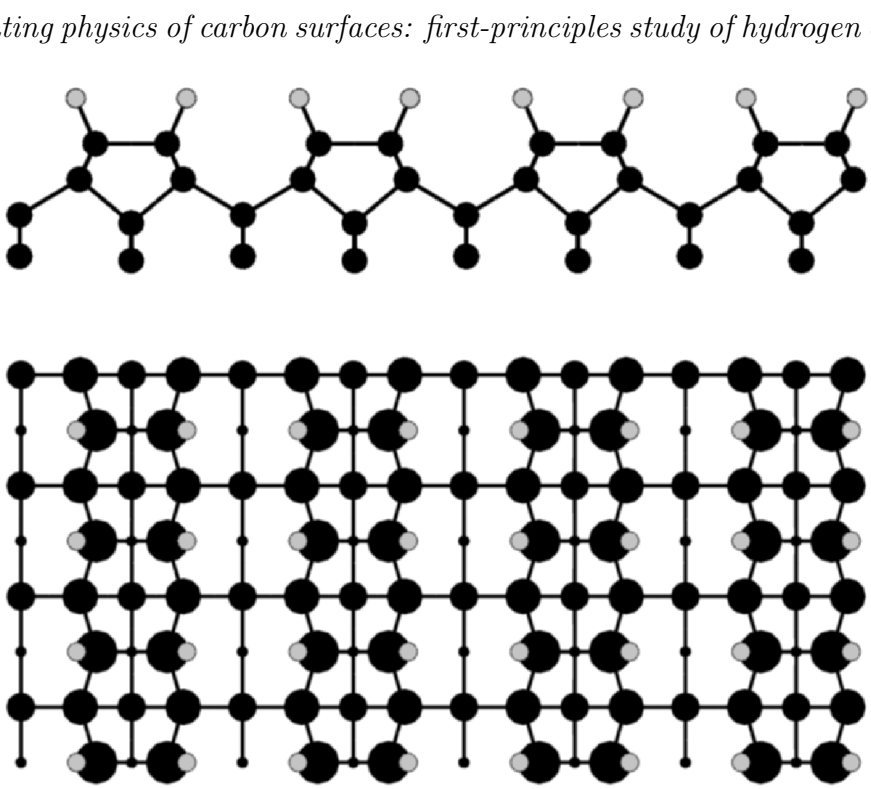

Figure 3. Side and top view of the monohydride C(001)2×1:H surface. Black balls represent C atoms, grey balls hydrogen atoms.

known stable phase for H covered C(001)2×1 surface under standard conditions [66] is the so called monohydride phase, where each surface C atom bonds an atomic H. DFT-based calculations [49, 67, 52] have shown that the hydrogenated surface is energetically favored (by 2.1 eV/atom) over the clean surface plus isolated H_2 gas-phase molecules. It is by now accepted that the 2×1 monohydride surface is the most stable form for the hydrogenated C(001), while the 1x1 dihydride is unstable due to steric repulsion between the hydrogen atoms [52]. In the monohydride phase, upon absorption of H, the surface dimers do not break, but they change from being double to single bonded. The C-C distance increases (1.61 Å, to be compared with 1.37 Å for the clean case). The agreement with LEED estimated C-C distance is excellent (1.60 Å[66]). A buckling of 0.18 Å and 0.10 Å is found at the 3rd and 4th layer, respectively, which slightly exceedes the experimental one from LEED experiments (0.08 and 0.06 Å[66]).

3.2.1. Electronic band structure The calculated electronic band structure is shown in Fig. 4. In agreement with previous calculations [49, 53], the adsorption of hydrogen causes the disappearance of the π and π^* states from the forbidden bulk gap region. Anyway surface states still appear in the fundamental gap, just below the bottom of the bulk conduction edge. These states are related to C-C and C-H bonds at the surface. In particular, (see Fig.5) if the lowest conduction state at Γ (LUMO, for simplicity) presents also some electron charge density above the surface, the LUMO+1 has almost all the weight of the electron wave function delocalized outside the surface, although

State	E_{LDA}	$\langle$HF$\rangle$	$\langle\Sigma_c\rangle$	$\langle v_{xc}^{LDA}\rangle$	$\langle$HF$\rangle$+$\langle\Sigma_c\rangle$-$\langle v_{xc}\rangle$	E_{GW}
HOMO	-0.60	-19.1	2.0	-16.5	-0.6	-1.1
LUMO	2.5	-2.3	-1.7	-5.0	1.0	3.4
LUMO+1	3.4	-0.3	-0.5	-0.7	0.1	3.6

Table 4. DFT and GW energies of single-particle states for the C(001)2×1:H surface [68]. The HOMO has bulk character, and the LUMO is a surface state related to C-C and C-H bonds, with also some weight above the surface. The LUMO+1 is a NFES. Also the exchange (HF) and correlation part of the self energy are shown. In comparison with Fig.4, the energy of the HOMO of the slab calculation lies 0.6 eV below the projected-bulk HOMO [49]. Energies in eV.

the state itself still lies (at least at the DFT level) below the vacuum. The LUMO+1 is a nearly-free electron state (NFES), and its behavior under GW correction is peculiar because of the delocalized nature of the electron wavefunction. In Tab. 4 we show the LDA-KS and the quasiparticle energies for some single-particle states at the Γ point, and the expectation value of the Hartree-Fock (HF) self-energy, of the correlation part of the self-energy (Σ_c), and of the of the exchange-correlation potential. HF is known to overestimate band-gaps in solids, and we will take into account these results only to analyze how much bare exchange is able to differentiate between the NFE state and the other conduction states. As a matter of fact from the third column of Tab. 4 we see that the LUMO+1 (NFE character) is significantly less affected by the HF corrections with respect to the LUMO state which is more localized within the bulk. This can be explained thinking that the overlap between the NFES wavefunction and the filled states wavefunctions is much smaller than the overlap of a LUMO-like state with the occupied states. Also the correlation term of Σ is much smaller (column 4). The overall effect is that the quasi-particle shift for the NFE state is one order of magnitude smaller than the quasi-particle shift of the other conduction states.

3.2.2. Electron Affinity As already mentioned, among the outstanding properties of diamond, its negative electron affinity is a unique characteristic not shared with any other semiconductors. NEA in diamond is stable in air up to several hundred Celsius degrees (see for example [2] and refs. therein).

The electron affinity χ of a system is defined as the amount of energy needed to get an electron from the conduction band out into the vacuum. Apparently the electron affinity seems a true bulk quantity which should not depend on surface orientation. However it is found that χ depends on the the surface from which the electron is extracted. In fact, besides band bending, the vacuum level which can be experimentally measured is not the *vacuum level at infinity* $E_{vac}(\infty)$, defined as the energy of an electron at rest at an infinite distance from the sample which is of course surface-invariant [3]; but the *vacuum level at the surface* $E_{vac}(S)$, defined as the energy of an electron at rest close to the surface, i.e. (following ref. [3]) at a distance larger than the inter-atomic

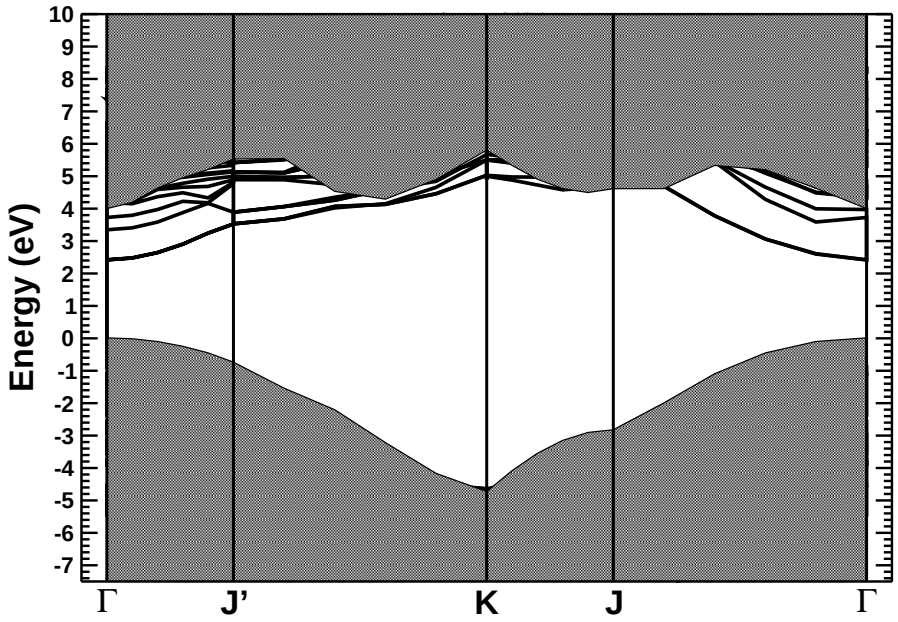

Figure 4. DFT band structure of the C(001)2×1:H surface. (Dots: surface bands; grey region: bulk projected).

distances but smaller than the size of the sample. This quantity is dependent on the specificity of the surface geometry and on the presence of different adsorbates. What is experimentally accessed is not the energy difference between the conduction band minimum and the vacuum level but the energy barrier that the electron must overcome in order to get into the vacuum. The existence of this energy barrier can be explained in terms of the presence of the interface alone: in fact, in an ideally truncated bulk, some of the surface electron will *spill out* into the vacuum creating a negative charge region just outside the solid; at the same time, the region just inside is left with a net positive charge. The total effect is thus the presence of an electric dipole at a microscopic level which gives rise to a potential which prevents other electrons to leave the solid [16]. Of course reconstructions and adsorbates strongly influence this microscopic dipole changing the potential barrier and thus the electron affinity. In particular the changes in χ due to the presence of adsorbates can be addressed very intuitively to differences in the electronegativity of the adsorbate atoms with respect to the substrate ones. The ability of the adsorbate atom to attract more (less) the electron, induces a polarization of the bond, which creates a negative (positive) charged region at the surface raising (lowering) χ. As a result, the presence of hydrogen lowers the energy barrier at the surface of diamond, and oxygen behaves in the exact opposite way; in fact the electron affinity of diamond can be tuned smoothly from its lowest to its maximum value by controlling the coverage of hydrogen and oxygen[17].

Many theoretical [49, 54, 61, 67, 55] and experimental ([17, 65, 55] and refs. therein) studies on the electron affinity of the C(001):H system have been carried out. Our results

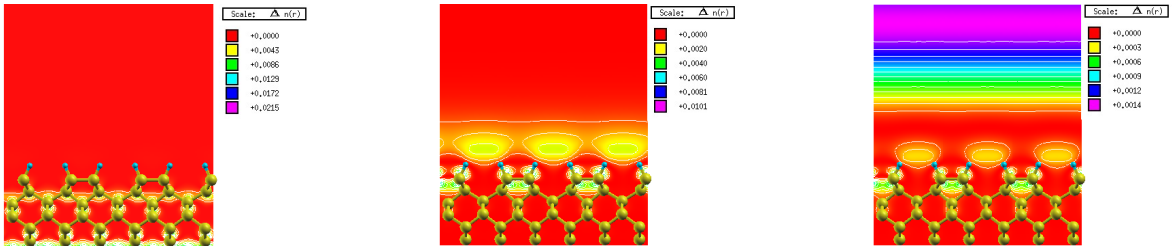

Figure 5. From left to right: Square modulus of the electronic KS wave function $|\psi(\mathbf{r})|^2$ of the HOMO, LUMO and LUMO+1 states at the C(001)2×1:H surface. The LUMO+1 state has a NFE character.

are shown in Tab. 3. DFT already predicts a negative EA (-0.7 eV). The inclusion of quasi-particle effects (GW) brings the EA to a more negative value (-1.5 eV), in good agreement with the experimental results of Ley (χ=-1.3 eV [17]), but quite too negative if compared with the values by [65] ($\sim$ -0.4 eV). Different surface preparation conditions and experimental techniques may explain the different affinity values reported in Tab. 3.

4. The C(111) surface

Cutting bulk diamond perpendicularly to the [111] direction can be done cutting either one or three sp^3 C-C bonds. The three dangling bonds surface has of course a much higher formation energy [69] and by cleavage only the single dangling bond surface can be obtained. All the results presented here hence concern the single dangling bond surface.

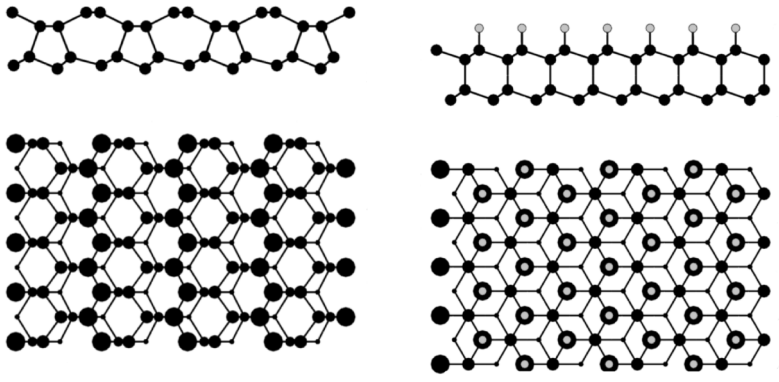

Figure 6. Left: side view (top panel), and top view (bottom panel), of the hydrogenated C(111) 1×1 surface. The single-dangling bond truncated bulk is obtained from such geometry with the removal of hydrogen. Right: side view (top panel), and top view (bottom panel), of the clean reconstructed C(111) 2×1 surface. Black balls represent C atoms, grey balls hydrogen atoms.

Right after cleavage the surface exhibits a 1×1 reconstruction. C(111)1×1 consists

	D	b(1)	b(2)	b(3)	b(4)	d_{23}	d'_{23}
EXP [79]	0.007	0.01	0.01	0.02	0.18	1.64	1.62
DFT-GGA	0.00	0.004	0.01	0.02	0.17	1.64	1.59

Table 5. Structural parameters of C(111) 2×1 obtained from LEED spot intensity vs voltage results [79], compared with DFT-GGA predictions. D is the degree of dimerisation; b(i) is the i-th layer buckling; d_{23} and d'_{23} are the lengths of the bonds connecting the 2^{nd} to the 3^{rd} atomic layer. All lengths are in Å. (From Ref. [82]

approximately of a truncated bulk with each dangling bond saturated by an hydrogen atom. The presence of hydrogen in the polished surface is confirmed by angle resolved photoemission spectra (ARPES) that show that in the 1×1 no occupied surface states are present [71, 72] within the fundamental gap. Also infrared-visible sum frequency generation spectroscopy has shown the presence of structures related to C-H bonds [73]. After annealing at more than 1100 K, hydrogen desorbs and the surface undergoes a 2×1 reconstruction. It is well accepted that the reconstruction geometry of this surface is the Pandey π-chain model [74], shown in Fig. 6. The reconstruction involves significant changes in the bonding of the atoms belonging to the first three layers, forming an almost one dimensional chain in the top layer. The Pandey chain reconstruction finds the most evident confirmation through the dispersion of the occupied surface states obtained by ARPES measurements [71, 75]. Besides that, also the great majority of experimental results, ranging from medium energy ion scattering [76, 77], LEED analysis of the spot intensity vs voltage [78, 79], X-ray diffraction structure analysis [80], confirm the Pandey model for the reconstruction of the (111) surface. As such diamond behaves in the same way as Si and Ge, which exhibit a Pandey-chain 2×1 reconstruction.
However the exact geometry of the unit cell is still controversial. While most of the theoretical study within DFT predict a non buckled non dimerised geometry [70], the situation on the experimental side is rather unclear. Dimerisation seems to be ruled out by ARPES experiment [75]; medium energy ion scattering data [76], X-ray diffraction structure analysis [80], and infrared-visible sum frequency generation measurements [73] find best agreement for an atomic arrangement featuring tilted chains, but can not completely rule out an unbuckled undimerized geometry. At the same time, core level binding-energy measurements [81], and a recent LEED study [79], show no evidence for buckling.

In Tab. 5 we show the structural parameters of the C(111) 2×1 Pandey-chain reconstruction obtained from a DFT total-energy minimization [82] compared to the LEED spot intensity vs voltage results [79]. As we can see the theoretical ground-state geometry is in excellent agreement with the experimental results. We can conclude that Diamond, Si, and Ge share the same model for the reconstruction of their (111) 2×1 surface, but, while in the case of Ge and Si the most stable geometry features tilted chains, diamond chains do not seem buckled [83].

4.1. Electronic band structure

Experimentally, direct photoemission experiments find occupied surface states within the fundamental gap. They show a strong dispersion along the chain direction and are almost flat perpendicularly to it [71, 75], consistently with a reconstruction model exhibiting one dimensional structures like the π bonded chains. There are also evidences of unoccupied surface states within the fundamental gap from two-photons photoelectron spectroscopy (2PPES) [84], high resolution soft X-rays absorption spectra [85], and electron energy loss spectroscopy (EELS) [81]. Finally a recently measured reflectance anisotropy spectrum [86, 87] shows an optical gap between surface states of ~ 1.5 eV.

The DFT electronic band structure of the clean C(111)(2×1) corresponding to the ground-state unbuckled undimerized geometry is shown in Fig. 7.

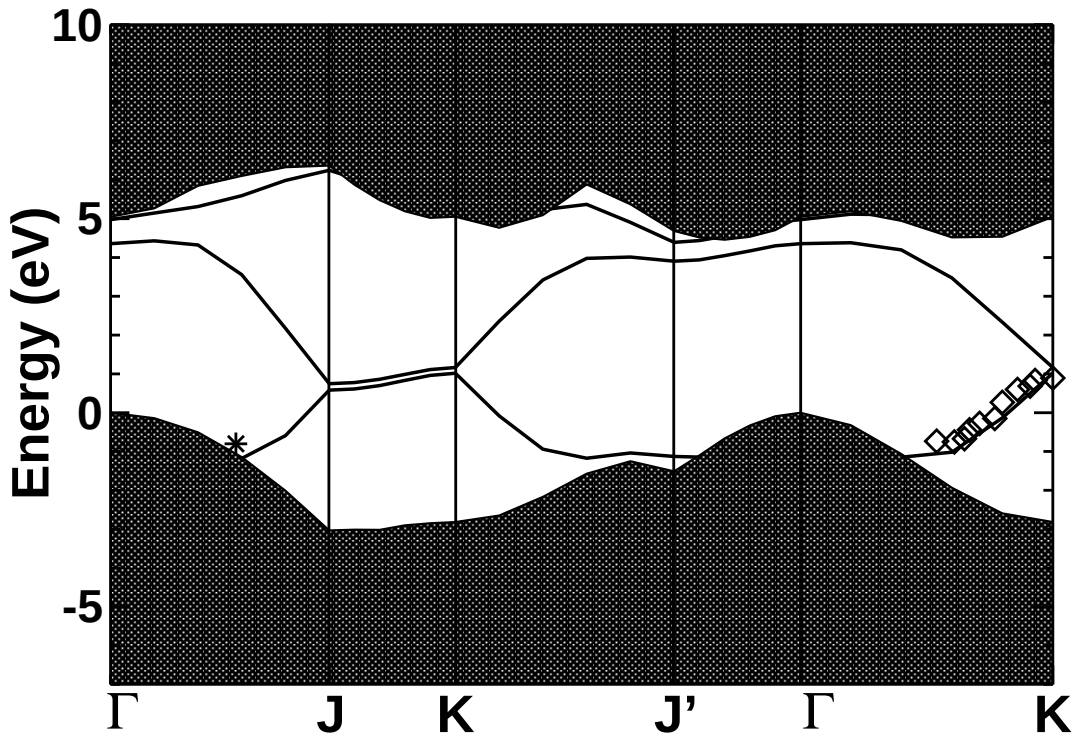

Figure 7. DFT-LDA electronic band structure of the C(111)2×1 surface. At the DFT level the surface is semimetallic.

The dispersion of the calculated bands seems to be in qualitatively good agreement with experimental data points. However, the surface is semi-metallic in contrast with experimental findings.

The degeneracy of the states along the JK line is strictly connected to the equivalence of the two atoms on the chain: if this equivalence is removed then the gap between surface states may open.

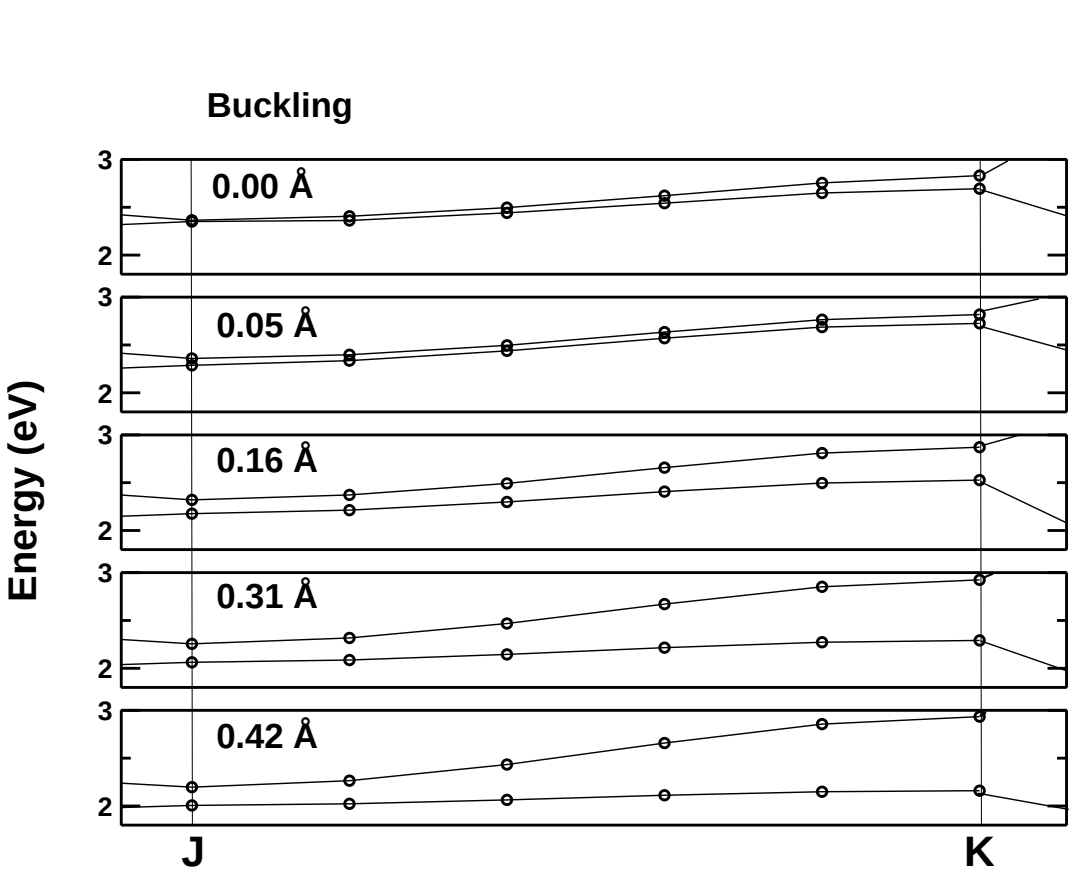

Figure 8. Electronic band structure of the 2×1 surface, along the JK directions for different values of the buckling of the surface chains. The degeneracy of the surface bands along the JK line is lifted by the presence of buckling. The upward dispersion of the bands, however, turns the surface semiconducting only in the case of a 0.42 Å buckling.

The two atoms on the chain are not equivalent taking into account the presence of the bulk, but evidently the difference is not enough to permit a strong energetic differentiation of the two. It is known that a lattice distortion, such as the buckling of the surface chains, provides Ge and Si of a semiconducting band structure.

Buckling $\mathring{A}$	Total Energy (Hartree)
0.00	0.000
0.05	+0.002
0.16	+0.017
0.31	+0.064
0.42	+0.110

Table 6. DFT total energies for the C(111)2×1 surface vs buckling.

If, starting from the fully relaxed geometry, we add an artificial buckling of the chain we can see how the electronic gap evolves. The results [82] are listed in Tab. 6 and Fig. 8. As we can see, only a strong (in terms of energy cost) buckling of 0.42 Å could induce an opening of the gap. The experimental values for the buckling range

between 0 (see for example [79]) and ~ 0.3 Å [80], and within this range the surface keeps being semimetallic.

A possible explanation to the absence of an electronic gap in the theoretical band structure of C(111) may be found in the application of DFT to the realm of electronic excitations, where it systematically underestimates electronic gaps. However, in the case of C(111)2×1 G_0W_0 fails to work [88]. As a matter of fact the G_0W_0 corrections do not change the situation because the two surface bands in the gap have almost identical character (dangling bond character) hence exchange and correlation effects do not differentiate among them. In the presence of some distortion, exchange and correlation effects would be different for one state with respect to the other, and a gap could open. But DFT does not find neither dimerization nor buckling. As such, there is no way, apart from having a different occupation number (which is not the case), by which exchange and correlation effects should distinguish between them.

The determination of the electronic band structure of C(111) requires then a more sophisticated treatment. A possibility is to search for a non-interacting Hamiltonian, different from the KS one, yielding a semiconducting starting point for the perturbative GW. This path has been explored in Ref. [89], where hybrid screened exchange (sX) functional [22, 57] and a Hartree Fock (HF) calculation have been performed. In

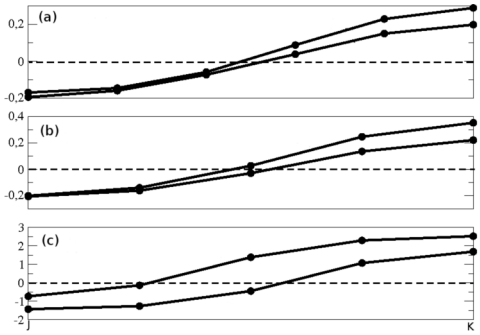

Figure 9. (From ref. [89]) C(111) surface states energies along the JK line, within the GGA, sX, and Hartree Fock schemes, for the equilibrium geometry (no buckling, no dimerisation). In all cases the surface is semimetallic. Note the different scales on the y axis. All energies are in eV and referred to the Fermi level.

Fig. 9 [89] the surface bands along the JK line , for the GGA, screened exchange and the Hartree-Fock calculations, are shown. In all the cases the surface keeps being semimetallic, and this is particularly amazing in the case of the Hartree-Fock results which is known to provide overestimated band gaps in solids.

The description of the semiconducting character of C(111) in absence of any buckling or dimerization has been finally achieved in ref. [88], through an iterative GW procedure. In that work, starting from an artificial population of the KS band structure, the eigenvalues in the expression of the self-energy have been updated until self-consistency is reached. The final band structure is reported in Fig. 10, a direct

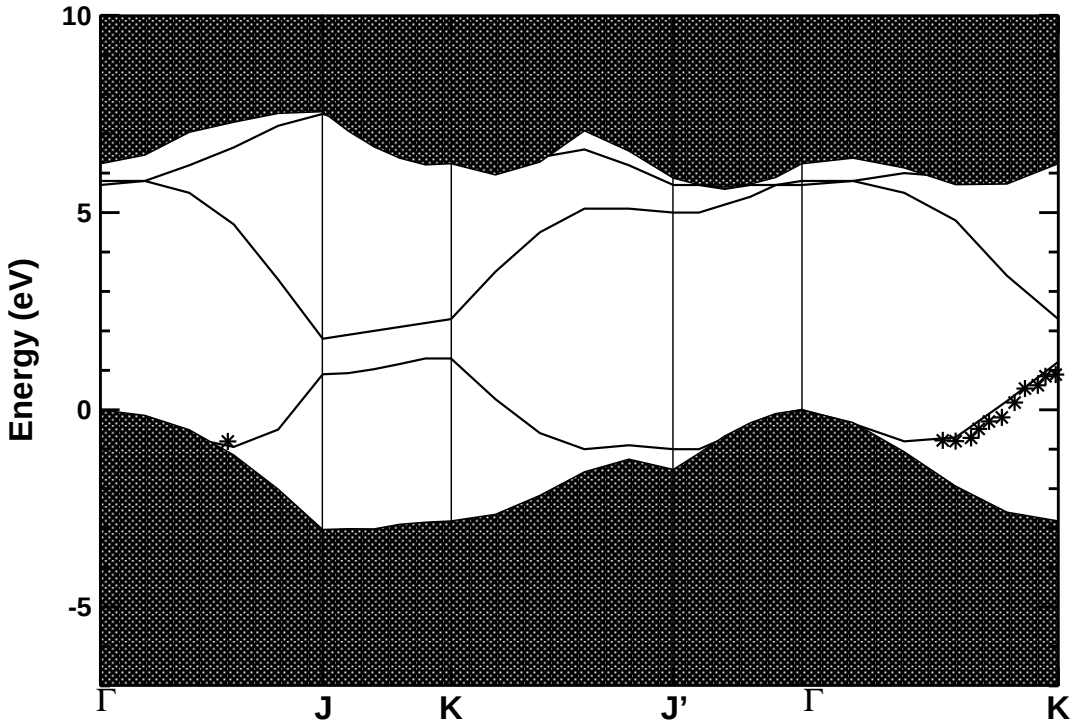

Figure 10. Electronic band structure of the C(111)2×1 surface within the self-consistent GW scheme. A gap of about 1 eV opens along the JK direction. Crosses: experimental results from [71, 75].

gap of about 1 eV has been found. While for the first time the semiconducting character of the surface has been recovered, the value of the electronic gap is still too small when compared with the experiments[86, 87]. Indeed, if ref. [88] proves that geometric distortions may not be necessary to open a gap in the band structure it shows, at the same time, that a quantitative description demands further studies, possibly investigating the effect of defects, adsorbates, better xc functionals, electron-phonon interactions etc... Also the calculated electron affinity χ_{GW}=0.8 eV (see Tab. 3, although well within the experimental range (0.38-1.5 eV [17] and ref. therein) points towards a strong distance between the theoretical surface model (clean, ideal) and the experimentally accessible, real, surface.

5. Hydrogenated C(111)

Right after cleavage the (111) face of diamond is H terminated. The surface is unreconstructed and the H atoms saturate the dangling bonds belonging to the C surface atoms pointing out in the [111] direction. The side and top view of the fully hydrogenated C(111) is presented in Fig. 6. Carbon preserves its sp^3 hybridization, the C-H bond length is 1.12 Å and the distance between the surface C atoms and the second layer ones is 1.52 Å, almost equal to the bulk C-C distance of 1.53 Å. As a

consequence of the different geometry, the electronic band structure of the hydrogen-terminated surface is completely different with respect to the clean one. As shown in

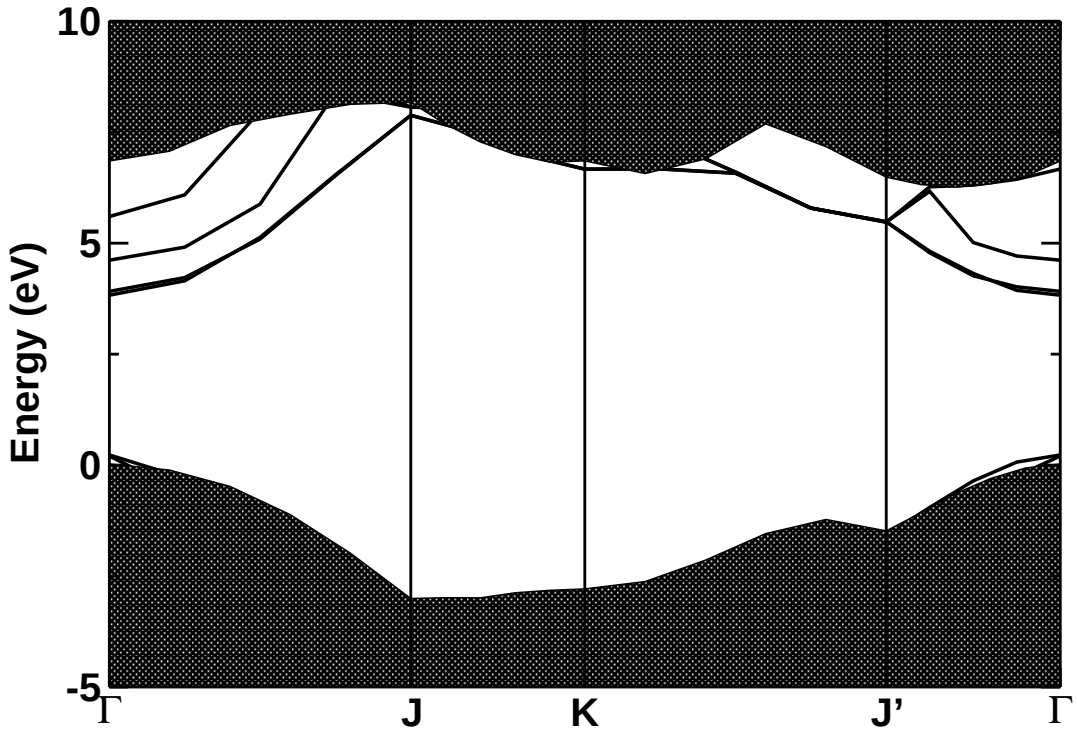

Figure 11. GW electronic band structure of the 1×1 C(111):H surface [90]. The 1×1 unit cell has been simulated within a 2×1 cell to be able to compare its band structure with the one of the clean 2×1 reconstructed surface.

Fig. 11, in the GW band structure empty surface states appear close to the Γ point right below the bulk conduction band minimum. Such states have a NFE character. In Fig. 12 we present the square modulus of the KS wave-function of the conduction band minimum at the Γ point (as before for brevity we will call this state the LUMO). The charge is strongly delocalized outside the surface. Also the LUMO+1 shares the same features, while the LUMO+2, for istance, is a bulk conduction state (see Fig. 12). The different nature of the conduction states at the Γ point results, as for the C(001)2×1:H surface, in different effects of many-body corrections to the energy of such single-particle states. A first probe of this different behaviour is given by the expectation value of the Hartree-Fock self-energy. In tab. 7 we show the LDA-KS and the quasiparticle energies for some single-particle states at the Γ point, and the expectation value of the Hartree-Fock (HF) self-energy, of the correlation part of the self-energy (Σ_c), of the of the exchange-correlation potential. From the third column of tab. 7 we see that the LUMO

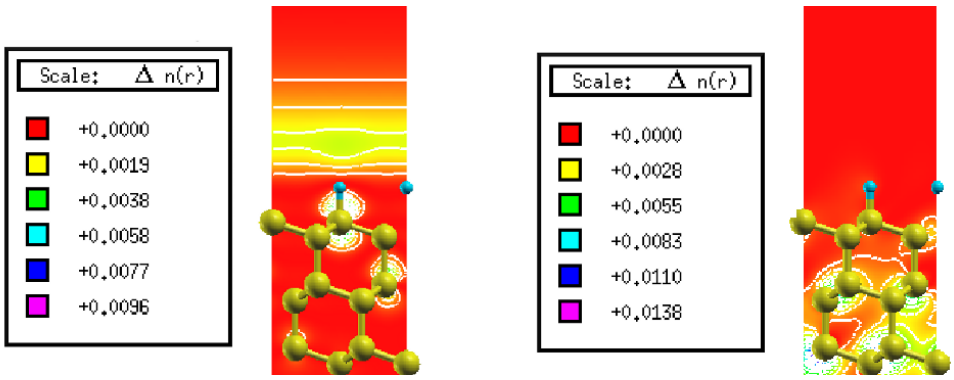

Figure 12. Square modulus of the single particle KS wavefunctions at the Γ point of the BZ for C(111):H. (Left) LUMO. The LUMO has a NFES character. (Right) LUMO+2. The LUMO+2 has a bulk character.

State	E_{LDA}	$\langle$HF$\rangle$	$\langle\Sigma_c\rangle$	$\langle v_{xc}^{LDA}\rangle$	$\langle$HF$\rangle+\langle\Sigma_c\rangle-\langle v_{xc}\rangle$	E_{GW}
HOMO	0.00	-19.21	1.94	-16.78	-0.49	-0.41
LUMO	2.75	-2.72	-2.03	-5.33	0.58	3.38
LUMO+2	4.85	-8.14	-4.23	-13.78	1.41	6.04

Table 7. DFT and GW energies of single-particle states for the C(111)2×1:H surface. The HOMO and LUMO+2 have bulk character, while the LUMO (and LUMO+1) is a NFES. Also the exchange (HF) and correlation part of the self energy are shown. All energies are in eV.

(NFE character) is significantly less affected by the HF corrections with respect to the LUMO+2 state which is localized within the bulk. Again, the overall effect is that the quasi-particle shift for the NFE state is much smaller than for the other conduction states, as in the case of the C(001)2×1:H surface (see tab.4).

In analogy with the (001) face, one of the most striking effect of hydrogen is that it turns the electron affinity of the surface to negative values. In tab. 3 the electron affinity of the clean and hydrogen-terminated (111) surfaces are compared. The change of the sign of the electron affinity upon hydrogenation is already present at the DFT level, and quasi-particle corrections further decrease the EA.

6. Graphane

Graphene, a honeycomb sheet of carbon atoms, is the first truely 2D system found in nature. Graphene appears in 0D, wrapped to form fullerens; in 1D, rolled in nanotubes; in 3D, stacked to form graphite. In recent years, graphene has become one of the most studied materials thanks to its unique physical properties. The amazing features of graphene range from the Dirac-like behavior of its electrons that gives rise to a

perfect conduction even in the presence of scatterers [93, 95], to its extreme mechanical properties, being the strongest material ever tested [96]. Its sensitivity to single adsorption events makes it an excellent candidate for chemical sensors. Graphene, a single monolayer of graphite, has a flat honeycomb lattice and its valence electron are sp^2 hybridized giving rise to a metallic band structure. The electronic properties of graphene have been the subject of a tremendous research effort both theoretically (for a review see ref. [97]) and experimentally (see ref. [93, 94]). For the purpose of this paper, i.e. the study of the effect of hydrogen absorption on the electronic properties of graphene, we need to mention only that graphene is a semimetal (or zero gap semiconductor) with the linearly dispersing bands crossing the Fermi level at the Dirac points (K and K' high-symmetry points of the hexagonal-lattice Brillouin zone). We leave the reader to the reviews cited above for further insights and information. Indeed, one of the greatest hindrance for the exploitation of graphene in electronic devices is the absence of a gap in its electronic structure. A possible way to engineer a gap, building new 2D crystals [93] upon periodic adsorbtion of different chemical species, has been proposed [98]. The first realization of such novel 2D crystals is graphane, a fully hydrogenated graphene sheet hypothesized in 2007 in Ref. [11], and then experimentally synthesized in 2008 [12, 13].

Upon the absorption of H a change of hybridization from sp^2 to sp^3 occurs and the sheet goes from a planar to a buckled geometry (see Fig. 13). Experimentally, a shrinking of the C-C bond [12] is found. Ab-initio calculations [11, 99], instead, find a widening of the C-C bond length from 1.42 Å (graphene) to 1.54 Å (graphane). The value of 1.54 Å corresponds to the C-C distance in bulk diamond, consistently with the sp^3 hybridization, whereas the value 1.42 Å is also the C-C bond length in graphite, consistently with the sp^2 hybridization. A possible explanation for this contradiction has been given by Legoas et al. [100] who have shown how breaking the H atoms up and down alternating pattern of ideal graphane, which is likely to happen in experiments, can lead to lattice contraction.

The effect of hydrogen passivation on the electronic structure of graphene is striking: all the dangling bonds are saturated and the sheet becomes semiconducting, as shown in Fig. 14. The metal-insulator transition, driven by H adsorption, occurs with an opening of a direct electronic gap at Γ as large as 6.1 eV (GW electronic gap). While the top of the valence band state is a C-C bonding state, the bottom of the conduction band exhibits a nearly-free-electron (NFE) character, as shown in Fig.15. The electronic density corresponding to this state is mainly delocalized above the carbon sheet [101], with possible important consequence in the transport properties of this material [102].

Many-body effects significantly influence the magnitude of the electronic gap of graphane [99, 103, 104]. Starting from a direct DFT gap at Γ of 3.5 eV, the GW corrections strongly increase its fundamental gap giving a quasi-particle gap of 6.1 eV (see table 8). Hence, graphene undergoes a metal-insulator transition upon hydrogen adsorption, with its electronic gap passing from zero (graphene) to 6.1 eV (graphane).

As already discussed, hydrogenated diamond surfaces have a negative EA.

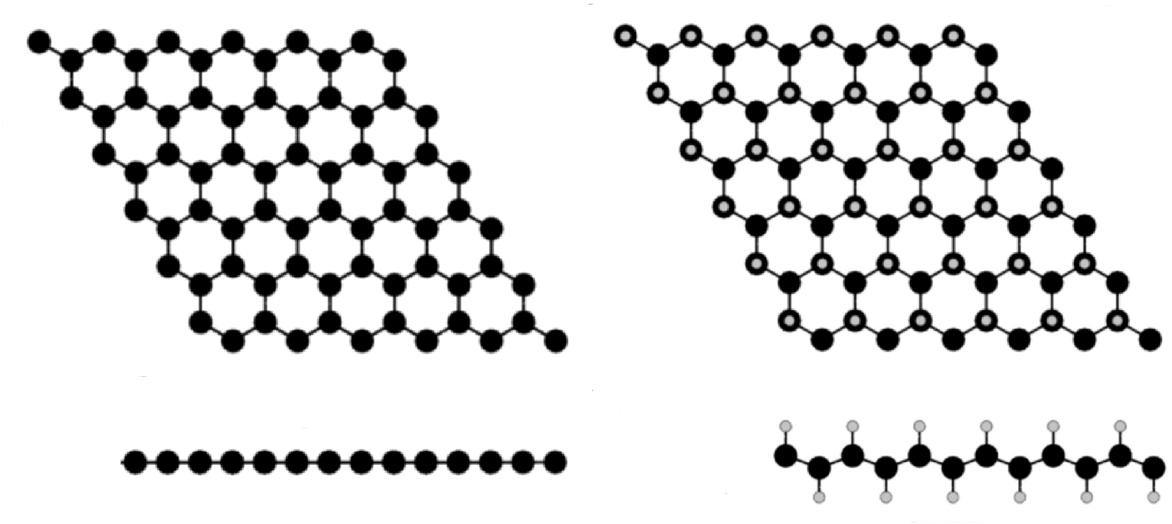

Figure 13. Graphene (left panel) and graphane (right panel) structures. Top view in the upper pictures and side view in the lower pictures.

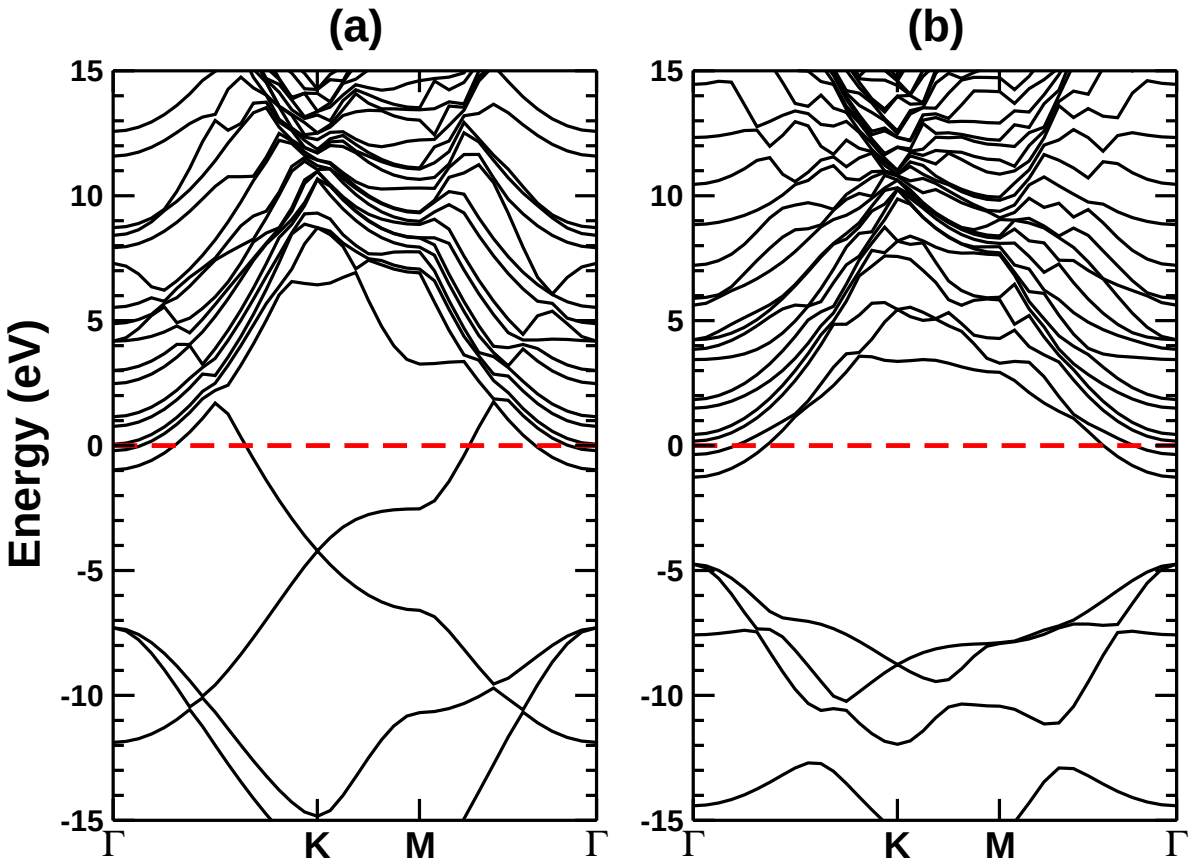

Figure 14. DFT electronic band Structure of Graphene (left panel) and graphane (right panel). Dashed lines indicate the vacuum level. In graphane the DFT gap at Γ opens to about 6.1 eV when many-body effects within GW are included.

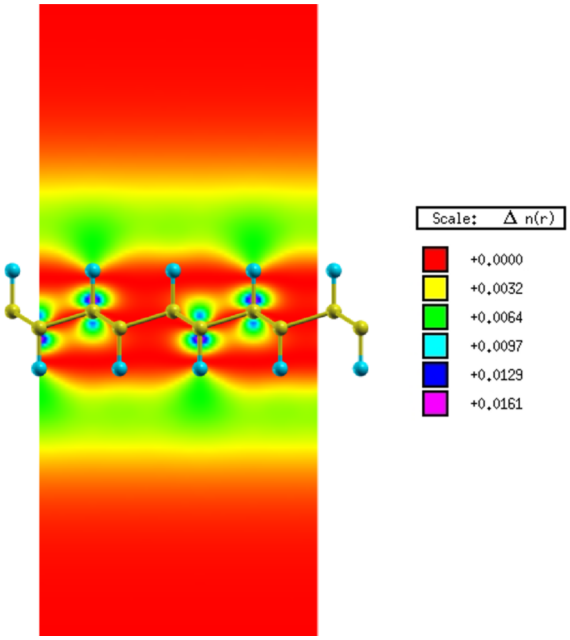

Figure 15. Squared modulus $|\phi(r)_{6,\Gamma}|^2$ of the wavefunction at Γ for the first empty state in graphane.

	Gap DFT	Gap GW	χ DFT	χ GW
Graphene	0 (K)	0 (K)	4.2	4.2
Graphane	3.5 (Γ)	6.1 (Γ)	1.2	0.4

Table 8. Minimum electronic gap and electron affinity for graphene and graphane, calculated within DFT and within GW. All energies are in eV.

Therefore, it is important to analyze whether this happens also in the case of graphene upon hydrogen uptake. As in the case of diamond surfaces, hydrogen lowers the EA of the carbon sheet, namely from 4.2 eV in the metallic phase (graphene) to 1.2 eV (DFT) in the insulator phase. Moreover, when self-energy effects are taken into account, the EA of graphane reaches a value close to zero ($\sim$0.4 eV, see table 8). Further and more refined calculations are envisaged to understand this point, and experimental verifications are needed .

7. Conclusions

In conclusion, we have presented ab-initio calculations on the effect of hydrogenation of diamond surfaces and of graphene. The geometrical structures, calculated within DFT-based methods, are reviewed. The electronic band structures with the inclusion of many-body effects are presented and discussed. Nearly free electron states seem to be characteristic of these systems. A negative electron affinity, fingerprint of the hydrogenated diamond surfaces, is well reproduced in our calculations, whereas we predict a small, though still positive electron affinity for graphane.

Acknowledgments

The authors whish to thank Dr. P. Gori and Dr. V. Garbuio for discussions concerning graphene and graphane, and with Prof. A. Shkrebtii, F. Bechstedt and R. Del Sole for C(001) and C(111) surfaces. CPU time granted by CINECA, ENEA CRESCO and CASPUR are gratefully acknowledged. The research leading to these results has received funding from the European Community's Seventh Framework Programme (FP7/2007-2013) under grant agreement no 211956.

References

[1] F. Bechstedt, A. A. Stekolnikov, J. Furthmüller, P. Käckell Phys. Rev. Lett. **87**, 16103 (2001).
[2] J. Ristein, Appl. Phys. A **82**, 377 (2006).
[3] D. Cahen, and A. Kahn Adv. Mater. **15**, 271 (2003).
[4] F. J. Himpsel, J. A. Knapp, J. A. VanVechten, and D. E. Eastman Phys. Rev. B **20**, 624 (1979).
[5] M. I. Landstrass and K. V. Ravi Appl. Phys. Lett. **55**, 975 (1989).
[6] F. Maier, M. Riedel, B. Mantel, J. Ristein, and L. Ley Phys. Rev. Lett. **85**, 3472 (2000).
[7] Y. Kuang, Y. Wang, N. Lee, A. Badzian, T. Badzian, and T. T. Tsong, Appl. Phys. Lett. **67**, 3721 (1995).
[8] R. E. Stallcup, II and J. M. Perez, Phys. Rev. Lett. **86**, 3368 (2001).
[9] M.-H. Tsai and Y.-Y. Yeh, Phys. Rev. B **58**, 2157 (1998).
[10] M. Schwitters, D. S. Martin, P. Unsworth, T. Farrell , J. E. Butler and P. Weightman, J. Phys.: Condens. Matter **21** 364218 (2009)
[11] J. O. Sofo, A. S. Chaudhari, and G. D. Barber Phys. Rev. B **75**, 153401 (2007).
[12] D. C. Elias, R. R. Nair, T. M. G. Mohiuddin, S. V. Morozov, P. Blake, M. P. A. C. Ferrari, D. W. Boukhvalov, M. I. Katsnelson, A. K. Geim, and K. S. Novoselov, Science **323**, 610 (2009).
[13] S. Ryu, M. Y. Han, J. Maultzsch, T. F. Heinz, P. Kim, M. L. Steigerwald, and L. E. Brus Nanoletters **8**, 4597 (2008).
[14] M. Posternak, A. Baldereschi, A. J. Freeman, E. Wimmer, and M. Weinert Phys. Rev. Lett. **50**, 761 (1983).
[15] The evaluation of the position of the bulk BCB with respect to the vacuum level is done performing an alignement of the slab and of the bulk average electrostatic potential energy following S. Baroni, R. Resta, A. Baldereschi, and M. Peressi in *Spectroscopy of Semiconductor Microsctructures*, edited by G. Fasol, A. Fasolino, and P. Lugli (Plenum, New York, 1989), pp 251-271
[16] L. Kronik, Y. Shapira Surf. Sci. Rep. **37**, 1 (1999).
[17] F. Maier, J. Reistein, and L. Ley Phys. Rev. B **64**, 165411 (2001).
[18] P. Hohenberg and W. Kohn, Phys. Rev. **136**, B864 (1964).
[19] *A primer in Density Functional Theory* Vol. **620** of *Lecture Notes in Physics*, edited by C. Fiolhais, F. Nogueira, and M. Marques (Springer, Berlin, 2003)
[20] W. Kohn and L. J. Sham, Phys. Rev. **140**, A1113 (1965).
[21] J. P. Perdew, J. A. Chevary, S. H. Vosko, K. A. Jackson, M. R. Pederson, D. J. Singh, and C. Fiolhais, Phys. Rev. B **46**, 6671 (1992).
[22] A. Seidl, A. G"orling, P. Vogl, J. A. Majewski, and M. Levy Phys. Rev. B **53**, 3764 (1996).
[23] M. Grüning, A. Marini, and A. Rubio Phys. Rev. B **74**, 161103 (2006).
[24] F. Fuchs, J. Furthmller, F. Bechstedt, M. Shishkin, and G. Kresse Phys. Rev. B **76**, 115109 (2007).
[25] J.P. Perdew, and A. Zunger Phys. Rev. B **23**, 5048 (1980).
[26] M. T. Czyźyk and G. A. Sawatzky Phys. Rev. B **49**, 14211 (1994).
[27] L.Fetter and J.D. Walecka *Quantum theory of Many Body Systems* , McGraw-Hill, New York, N.Y.

1981 R. D. Mattuck, *A guide to Feynman diagrams in the many body problem* , McGraw-Hill, New York (1976).
[28] P.M.Echenique, J.M.Pitarke, E. V. Chulkov and A. Rubio , *Chemical Physics* **251**, 1 (2000).
[29] L. Hedin and B.J. Lundquist in Solid State Physics. edited by H. Ehrereich, F. Seitz and D. Turnbull (Academic press, New York, N.Y. 1969), Vol **23**, p. 1.
[30] M.S. Hybertsen, S.G. Louie, Phys. Rev. B 34, 5390 (1986).
[31] O. Pulci et al. *Phys. Rev. B* **60** , 16758 (1999).
[32] Landolt-Börnstein, *Numerical Data and Functional Relationships in Surface Science and Technology*, New Series Vol. 17a, Ed. O. Madelung, Springer-Verlag, Berlin,(1982).
[33] T. Kotani, M. van Schilfgaarde, and S. V. Faleev Phys. Rev. B **76**, 165106 (2007).
[34] M. Lopez del Puerto, M.L. Tiago, and J.R. Chelikowsky, Phys. Rev. B **77**, 045404 (2008).
[35] O. Pulci, L. Reining, G. Onida, R. Del Sole, F. Bechstedt, Comp. Mat. Sci. **20**, 300 (2001).
[36] J. C. Grossman, M. Rohlfing, L. Mitas, S.G. Louie, and M. L. Cohen, Phys. Rev. Lett. **86**, 472 (2001).
[37] J.L. Li, G.M. Rignanese, E.K. Chang, X. Blase, and S.G. Louie, Phys. Rev. B **66**, 35102 (2002).
[38] F. Bruneval, N. Vast, L. Reining, M. Izquierdo, F. Sirotti, and N. Barrett, Phys. Rev. Lett. **97**, 267601 (2006).
[39] Fabien Bruneval, Nathalie Vast, and Lucia Reining Phys. Rev. B **74**, 045102 (2006).
[40] F. Bruneval, F. Sottile, V. Olevano, R. Del Sole, and L. Reining Phys. Rev. Lett.**94**, 186402 (2005).
[41] M. Gatti, F. Bruneval, V. Olevano, and L. Reining, Phys. Rev. Lett. **99**, 266402 (2007).
[42] B.B. Pate Surf. Sci., **165**, 83 (1986).
[43] B.D. Thoms and J. E. Butler, Surf. Sci. **328**, 291 (1995).
[44] D. J. Chadi, Phys. Rev. Lett. **43**, 43 (1979).
[45] J.A. Kubby et al. Phys. Rev. **B 36** 6079 (1987)
[46] M. Palummo, O. Pulci, A. Marini, L. Reining, and R. Del Sole, Phys. Rev. B **74**, 235431 (2006).
[47] M.D. Winn and M. Rassinger and J. Hafner, Phys. Rev. B, **55**,5364 (1997).
[48] Z. Zhang and M. Wensell and J. Bernholc Phys. Rev. B **51**, 5291, (1995).
[49] S. J. Sque, R. Jones, and P. R. Briddon Phys. Rev. B **73**, 085313 (2006).
[50] P. Krüger and J. Pollmann, Phys. Rev. Lett. **74**, 1155 (1995).
[51] M. Palummo, O. Pulci, R. Del Sole, A. Marini, M. Schwitters, S. R. Haines, K. H. Williams, D. S. Martin, P. Weightman, and J. E. Butler, Phys. Rev. Lett. **94**, 087404 (2005).
[52] For a comparison with other DFT calculations, see for example H. Tamura et al. Phys. Rev. **B 61**,11025 (2000).
[53] C. Kress, M. Fiedler, W. G. Schmidt, and F. Bechstedt Phys. Rev. B **50**, 17697 (1994).
[54] M. J. Rutter and J. Robertson Phys. Rev. **B 57**, 9241 (1998)
[55] J. van der Weide et al. Phys. Rev. **B 50**, 5803 (1994)
[56] R. Graupner, F. Maier, J. Ristein, L. Ley, and Ch. Jung Phys. Rev. B **57**, 12397 (1998).
[57] sX calculations have been performed using the VASP code. The inverse screening k_{TF} has been selected as $k_{TF} = 0.9$ Å^{-1} for best fit with the GW calculations in the C(001)2×1 case. For the C(111)2×1 surface, no value of k_{TF} able to open a gap was found.
[58] C. Noguez, O. Pulci, 'Quantum Mechanical Calculations of Electronic and Optical Properties of Semiconductor Surfaces', chap. 12 of the book 'Quantum Chemical Calculations of Surfaces and Interfaces of Materials', ISBN: 1-58883-138-8, American Scientific Publishers, Vladimir A. Basiuk and Piero Ugliengo Eds., Pages: 217-248 (2009)
[59] P. K. Baumann, R. J. Nemanich Surf. Sci., **409**, 320 (1998).
[60] L. Diederich, O. M. Küttel, P. Aebi, L. Schlapbach Surf. Sci., **418**, 219 (1998).
[61] J. Robertson, M. J. Rutter, Diam. Rel. Mat. **7**, 620 (1998).
[62] J.B. Cui, J. Reistein, and L. Ley Phys. Rev. Lett. **81**, 429 (1998)
[63] This work
[64] C. Bandis and B. B. Pate Phys. Rev. B **52**, 12056 (1995).
[65] T. P. Humphreys, R. E. Thomas, D. P. Malta, J. B. Posthill, M. J. Mantini, R. A. Rudder, G. C.

Hudson, R. J. Markunas, and C. Pettenkofer Appl. Phys. Lett. **70**, 1257 (1997).
[66] Y. M. Wang, K. W. Wong, S. T. Lee, M. Nishitani-Gamo, I. Sakaguchi, K. P. Loh, T. Ando Diam. and Rel. Mat., **9**, 1582 (2000).
[67] J. Furthmüeller, J. Hafner, and G. Kresse, Phys. Rev. **B 53**, 7334 (1996)
[68] DFT and GW calculations on the C(001)2×1 surface have been performed using a 12 C-layer slab (24 carbon atoms), terminated on the top and on the bottom layer with H, leaving about 20 Å vacuum between image slabs. The geometry has been relaxed till the forces were below 0.5×10^{-3}eV/Å. An energy cutoff of 45Ry has been used. The RPA screening and the correlation part of the Self-Energy Σ_c has been calculated using 3057plane waves and 500 bands. A plasmon pole approximation has been used. For the exchange part of the Self-Energy Σ_x we have used 7999 plane waves.
[69] A. Scholze, W. G. Schmidt, and F. Bechstedt Phys. Rev. B 53, (1996).
[70] F. Bechstedt, *'Principles of Surface Physics'*, Springer (2003).
[71] F.J. Himpsel, D.E. Eastman, P.Heimann, J.F. van der Veen, Phys. Rev. B **24**, 7270 (1981).
[72] B.B. Pate, P.M. Stefan, C. Binnis, P.J. Jupiter, I. Lindau, and W.E. Spicer J. Vac. Sci. Technol. **19**, 349 (1981).
[73] R.P. Chin, J.Y. Huang, Y.R. Shen, T.J. Chuang, and H. Seki Phys. Rev. B **52**, 5985 (1995).
[74] K.C. Pandey, Phys. Rev. B **25**, R4338 (1982)
[75] R. Graupner et al., Phys. Rev. B **55**, 10841 (1997).
[76] W.J. Huisman, J.F. Peters, J.F. van der Veen, Surf. Sci. **396**, 253 (1998).
[77] T.E. Derry, L. Smit, and J.F. Van Der Veen Surf. Sci. **167**, 502 (1986).
[78] E.C. Sowa, G.D. Kubiak, R.H.Stulen, and M.A. VanHove J. Vac. Sci. Technol. A **6**, 832 (1988).
[79] S. Walter, J. Bernhardt, U. Starke, K. Heinze, F. Maier, J. Ristein, and L. Ley J. Phys. Condens. Matter **14**, 3085 (2002).
[80] W.J. Huisman, et al., Surf. Sci. **396**, 241 (1998).
[81] J.F. Morar, F.J. Himpsel, G. Hollinger, J.L. Jordon, G. Hughes, and F.R. McFeely, Phys. Rev. B **33**, 1340 (1985).
[82] O. Pulci, M. Marsili, P. Gori, M. Palummo, A. Cricenti, F. Bechstedt, R. Del Sole, Appl. Phys. A,**85**,361 (2006).
[83] A.A. Stekolnikov, J. Furthmüller, and F. Bechstedt Phys. Rev. B **65**, 115318 (2002).
[84] G. D. Kubiak, and K. W. Kolasinski Phys. Rev. B **39**, 1381 (1989).
[85] J.F. Morar, F.J. Himpsel, G. Hollinger, J.L. Jordon, G. Hughes, and F.R. McFeely, Phys. Rev. B **33**, 1346 (1985).
[86] G. Bussetti, C. Goletti, A. Violante, P. Chiaradia, and T. Derry, Superlatt. and Microstr. **46**, 227 (2009).
[87] G. Bussetti, et al., Europhys. Lett. **79**, 57002 (2007).
[88] M. Marsili, O. Pulci, F. Bechstedt, and R. Del Sole Phys. Rev. B 72, 115415 (2005).
[89] M. Marsili, O. Pulci, F. Fuchs, F. Bechstedt, and R. Del Sole, Surf. Sc., **601**, 4097 (2007).
[90] DFT and GW calculations on the C(111):H surface have been performed using a 12 C-layer slab (24 carbon atoms), terminated on the top and on the bottom layer with H, leaving about 13.5 Å vacuum between image slabs. The geometry has been relaxed till the forces were below 0.5×10^{-3}eV/Å. An energy cutoff of 45Ry has been used. We used the pseudopotentials C.pz-vbc.UPF and H.pz-vbc.UPF from http://www.quantum-espresso.org. The RPA screening and the correlation part of the Self-Energy Σ_c has been calculated using 1500plane waves and 500 bands. A plasmon pole approximation has been used. DFT calculations have been performed with the PWSCF code [91], while GW calculations with the Yambo code [92].
[91] P. Giannozzi, *et al.*, J.Phys.:Condens.Matter, 21, 395502 (2009).
[92] A. Marini, C. Hogan, M. Grüning, D. Varsano, Comp. Phys. Comm. **180**, 1392 (2009).
[93] A. K. Geim Science, **324**, 1530 (2009).
[94] M. J. Allen, V. C. Tung, and R. B. Kaner, Chem. Rev. **110**, 132 (2010)
[95] T. Ando, NPG Asia Mater. **1**, 17 (2009).

[96] C. Lee, X. Wei, J. W. Kysar, J. Hone, Science, **321**, 385 (2008).
[97] A. H. Castro Neto, F. Guinea, N. M. Peres, K. S. Novoselov, A. K. Geim, Rev. Mod. Phys. **81**, 109 (2009).
[98] D. W. Boukhvalov, and M. I. Katsnelson J. Phys.: Condens. Matter **21**, 344205 (2009).
[99] O. Pulci, P. Gori, M. Marsili, V. Garbuio, A. P. Seitsonen, F. Bechstedt, A. Cricenti and R. Del Sole, Phys. Status Solidi A, 19 (2010) DOI 10.1002/pssa.200982503
[100] M Z S Flores et al., Nanotechnology **20**, 465704 (2009).
[101] N. Lu, Z. Li, J. Yang, J. Phys. Chem. C , **113**, 16741-16746 (2009).
[102] S. Okada, A. Oshiyama, and S. Saito Phys. Rev. B **62**, 7634 (2000).
[103] S. Lebégue, M. Klintenberg, O. Eriksson, and M. I. Katsnelson, Phys. Rev. B **79**, 245117 (2009).
(
[104] P. Gori, M. Marsili, V. Garbuio, and O. Pulci, in preparation).